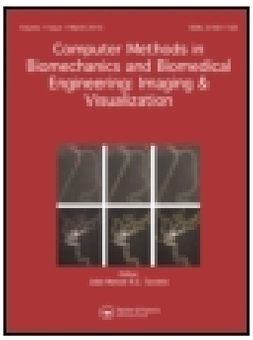

Taylor & Francis
Taylor & Francis Group

Computer Methods in Biomechanics and Biomedical Engineering: Imaging & Visualization

ISSN: 2168-1163 (Print) 2168-1171 (Online) Journal homepage: https://www.tandfonline.com/loi/tciv20

An automatic level set method for hippocampus segmentation in MR images

Nazanin Safavian, Seyed Amir Hossein Batouli & Mohammad Ali Oghabian

To cite this article: Nazanin Safavian, Seyed Amir Hossein Batouli & Mohammad Ali Oghabian (2019): An automatic level set method for hippocampus segmentation in MR images, Computer Methods in Biomechanics and Biomedical Engineering: Imaging & Visualization, DOI: 10.1080/21681163.2019.1706054

To link to this article: https://doi.org/10.1080/21681163.2019.1706054

Published online: 26 Dec 2019.

COMPUTER METHODS IN BIOMECHANICS AND BIOMEDICAL ENGINEERING: IMAGING & VISUALIZATION
https://doi.org/10.1080/21681163.2019.1706054

An automatic level set method for hippocampus segmentation in MR images

Nazanin Safavian[a,b], Seyed Amir Hossein Batouli[a,c] and Mohammad Ali Oghabian[a,d]

[a]Neuroimaging and Analysis Group (NIAG), Tehran University of Medical Sciences, Tehran, Iran; [b]Department of Biomedical Engineering, Science and Research Branch, Islamic Azad University, Tehran, Iran; [c]Department of Neuroscience and Addiction Studies, School of Advanced Technologies in Medicine, Tehran University of Medical Sciences, Tehran, Iran; [d]Medical Physics and Biomedical Engineering Department, Tehran University of Medical Sciences, Tehran, Iran

ABSTRACT

Hippocampus segmentation in MR images is beneficial for the diagnosis of many diseases and pathologies such as Alzheimer's disease. Manual segmentation of the hippocampus is highly time-consuming and has low reproducibility; however, automated methods have introduced substantial gains in this regard. In this study, we used a novel level-set method for hippocampus segmentation in combination with the SBGFRLS (Selective Binary and Gaussian Filtering Regularised Level Set) and LAC (Localising Region-Based Active Contours) algorithms. The proposed method avoided the algorithms which required a large database and instead used a more complex level set approach to obtain comparable accuracy. This method was applied to a set of 36 MRI scans provided by the Alzheimer's Disease Neuroimaging Initiative (ADNI), using the Harmonised Hippocampal Protocol (HarP) as the gold standard. In addition, the results were compared with the outputs of the Freesurfer software package. In regards to the similarity indices, the results of our algorithm (mean Dice = 0.847) were more comparable with the gold standard compared to those of Freesurfer. Classification results for AD vs control and MCI vs control showed a high degree of accuracy (91% and 75%, respectively). Therefore, this method can be an option for accurate and robust segmentation of the hippocampus.

ARTICLE HISTORY
Received 16 June 2018
Accepted 14 December 2019

KEYWORDS
Hippocampus; segmentation; magnetic resonance imaging; level-set; HarP

1. Introduction

The morphological analysis of brain structures in medical images, such as in Magnetic Resonance Imaging (MRI), non-invasively provides information about the shape and volume of the brain structures. This has many applications in disease diagnosis, therapy procedures and surgical planning. One of the most important subcortical brain structures is the hippocampus. It is involved in many functions such as memory, spatial navigation, learning, regulation of hypothalamic functions and emotional behaviour. The abnormality of this structure is thought to be associated with neurodegenerative diseases and brain disorders such as Alzheimer's disease, mild cognitive impairment, traumatic brain injury, schizophrenia, epilepsy and major depression (Geuze et al. 2005). In cases of schizophrenia, Alzheimer's disease, epilepsy and among other conditions the shape of hippocampus is altered and could be used as one of the indicators (Csernansky et al. 1998; van leemput et al. 2009). In addition, it is one of the few brain regions in which neurogenesis occurs (Anand and Dhikav 2012). As a result, clear segmentation of this structure in MRI is valuable.

The current gold standard for hippocampus segmentation in MRI is manual delineation of the structure's borders in each slice by a specialist. This procedure is time-consuming and it is subject to low reproducibility, as the final result is dependent on the inputs provided by the user which leads to high inter-rater (performed by different users) and intra-rater (performed by the same user in different moments) variability. To overcome these issues, automated and semi-automated methods have been proposed for hippocampus segmentation. These methods also face challenges such as low contrast of the MRI and existence of neighbouring structures with similar intensity, small size and complex shape of hippocampus, and its fuzzy and discontinuous boundaries.

In the early 1990s, semi-automated methods which required user interaction were introduced. This interaction was a major drawback of those algorithms as it caused low reproducibility, and was also time-consuming. For instance, some markers on the border of hippocampus defined by the user were used in registration step (Haller et al. 1997; Shen et al. 2002). Later, these semi-automated methods were able to reach higher reproducibility by limiting the level of the user interaction, for example, by only determining one central seed-point (Chupin et al. 2007). Fully automated methods began being proposed in the early 2000s in order to overcome these limitations, and they fall into three categories.

(I) Atlas-based methods are the first category. These can be single-atlas, multi-atlas or probabilistic-atlas techniques. The accuracy of the single-atlas technique was limited to the quality of the atlas as well as the registration process. One recent study tried to optimise the registration process by using a graph cut algorithm (Boykov et al. 2001), which increased the accuracy of

CONTACT Mohammad Ali Oghabian oghabian@sina.tums.ac.ir Neuroimaging and Analysis Group (NIAG), Research Center for Cellular and Molecular Imaging (RCMCI), Tehran University of Medical Sciences (TUMS), Tehran, Iran

segmentation (Kwak et al. 2013). One of the first multi-atlas implementations was proposed by (Heckemann et al. 2006). In the multi-atlas approach, the target image was registered to multiple atlases, and using the label fusion technique (Robitaille and Duchesne 2012), the final segmentation was provided (Platero and Tobar 2017). In (Khan et al. 2011) which is a multi-atlas method, dynamic information and supervised classifier were combined and were used for atlas selection. Using local similarity metrics (Akhondi-asl et al. 2011; Cardoso et al. 2013) in hippocampus to select the optimum atlases, can improve final results. To produce more accurate segmentation especially in the case of pathology (Heckemann et al. 2010) proposed incorporating tissue classification algorithm into the registration procedure. In (Collins and Pruessner 2010), three atlas-based methods were evaluated including ANIMAL (Automatic Nonlinear Image Matching and Anatomical Labelling) which is a single atlas method using non-linear registration, described in (Collins and Evans 1997). An optimised pipeline for multi-atlas segmentation which considered both accuracy and computational time was introduced in (Lötjönen et al. 2010) and a novel approach to reduce the number of atlases used was proposed in (Pipitone et al. 2014). According to (Dill et al. 2015), for segmenting the hippocampal subfields the major approaches are multi-atlas techniques (Yushkevich et al. 2010; Pipitone et al. 2014). As it was mentioned previously, final segmentation in multi-atlas methods is created through label fusion techniques. For instance, a new label fusion method was proposed by (Hao et al. 2014) applying statistical learning technique. One of the other label fusion techniques is a patch-based method which was first proposed in (Coupé et al. 2011), and can be categorised as a dictionary-learning problem. According to (Zandifar et al. 2017) which compared some automated hippocampus segmentation methods on the same dataset, the most promising method was patch-based method with non-linear registration and error correction technique; although it should be taken into account that a small patch may not be an optimum descriptor for the whole structure. Another recent work which integrated the random forest regression-based multi-atlas method and pattern recognition-based label fusion technique is described here (Zheng and Fan 2018). In probabilistic-atlas methods, the atlases were registered into a standard space in order to make the algorithm capable of computing the probabilities of occurrence of each label in each voxel through consideration of image intensities and local and global positions. Next, classification framework was applied which utilised these probabilities to obtain the final segmentation (Tong et al. 2013; Kim et al. 2013). A combination of probabilistic atlas and anatomical landmarks was proposed for hippocampus segmentation by (Chupin et al. 2009) which is robust to changes in acquisition parameters. In general, atlas-based approaches provide robust segmentation results; however, the registration procedure in these algorithms is computationally expensive, especially in multi-atlas methods.

(II) The second category is related to machine learning techniques, especially the Artificial Neural Networks (ANN), which have excellent performance in segmenting brain structures (Dolz et al. 2015). As an example, the ANN approach was used to segment the hippocampus in T1- and T2-weighted MR images (Hult 2003). In (Amoroso et al. 2015) a novel hippocampus segmentation method called Hippocampal Unified Multi-Atlas-Networks (HUMAN) was proposed which combined multi-atlas technique with ANN and used optimal atlases to train their network to obtain final segmentation. In the past few years, deep learning techniques and in particular the Convolution Neural Network (CNN) were also used for this aim (Lecun et al. 1998). One of the benefits of CNN in comparison with fully connected networks is that there are fewer parameters to estimate and therefore the training is easier. A recent study that used CNN for hippocampus segmentation (Bao and Chung 2018) proposed a novel architecture by the name of Multi-scale structured CNN (MS-CNN) to overcome problems such as complex background and similar histogram profiles in the MR images. Additionally, they applied a dynamic random walker approach to smooth the final borders of the hippocampus. Despite the high accuracy, some drawbacks of these approaches are heavy algorithm design, difficulty of understanding the structure of the algorithm, and increased risk of over-fitting.

(III) The third category is deformable models, such as the Active Contour Models (ACM) (Kass et al. 1988), in which the main idea is to iteratively deform a contour according to the statistical information of intensity, image gradient, or both, and to stop the contour at the borders of the desired object. These are generally categorised as region or edge-based deformable models. Level-set, an energy minimisation framework that enables an algorithm to naturally follow the topological changes (Sethian 1999), is one of the most important approaches for deformable models. Geodesic active contour (GAC) (Caselles et al. 1997) is the most popular edge-based level-set model, as well as the Chan-Vese (Chan and Vese 2001) as a region-based model. Recent level-set methods allow integration of both prior information and image information in one single optimisation framework, which is essential for hippocampus segmentation. An Adaptive Gradient Distribution Boundary map (AGDB), which controls the weight of contributed image and prior information in an ACM framework energy minimisation was previously proposed (Zarpalas et al. 2013). This method was later improved by proposing OLMs (Optimal Local Maps) for controlling the contribution of prior, edge and region information by local weighting in the ACM framework (Zarpalas et al. 2014); however, due to the training step and extraction of OLMs as well as its multi-atlas approach, this method has a high computational load. Others intended to decrease the computational load by using an alternative

approach to compute the prior information and locally integrate it into the conventional GAC model (Achuthan and Rajeswari 2015).

As a result, in this study, a novel approach for hippocampus segmentation is proposed which can be categorised in the third group mentioned above. We obtained prior information from an affine registration, followed by a non-linear registration step. Then, we locally integrated this information using a binary weighting map of image gradient information into an innovative level-set framework which adaptively uses local and global region information of the target image. As our method does not need training or multiple registration steps, the computational load is decreased. The results of the proposed method were compared with the results of the manual segmentation of the hippocampus as well as with the segmentation results of the Freesurfer software package.

2. Materials and methods

2.1. Dataset

We used the MRI data from the Alzheimer's Disease Neuroimaging Initiative (ADNI, http://adni.loni.usc.edu) database (Jack et al. 2008). Thirty-six images, whose ground truth segmentations according to the Harmonised Hippocampal Protocol (HarP) were available (Apostolova et al. 2015; Boccardi et al. 2015a), were randomly selected including normal control (NC), mild cognitive impairment (MCI) and Alzheimer's disease (AD). A summary of the selected data is provided in Table 1.

2.2. Manual segmentation

With the goal of creating a standard manual segmentation protocol for hippocampus on MR images, the Harmonised Hippocampal Protocol (HarP) was introduced (http://www.hippocampal-protocol.net). A previous study validated the HarP protocol with the aid of many clinical and educational centres (Frisoni et al. 2015). The study showed that it has a higher stability compared to local manual segmentation protocols. They concluded that HarP could be a reference and unified protocol for hippocampus segmentation, and as a result, this protocol was used as the gold standard here. The manual segmentation for our dataset was provided by five qualified HarP tracers whose absolute interrater interclass correlation coefficients were 0.95 and 0.97 for left and right hippocampus, respectively (Boccardi et al. 2015b).

2.3. Freesurfer segmentation

Freesurfer (http://surfer.nmr.mgh.harvard.edu/), a well-known and freely available software for subcortical segmentation and cortical parcellation, has become an accepted reference in brain structure segmentation. In summary, the details of subcortical segmentation algorithm in Freesurfer are as follows: 1) an atlas from a training set, whose brains are manually labelled and mapped into MNI305 common space, is used in an automated segmentation procedure; 2) three types of probabilities are calculated at each point in the atlas: a) the probability of belonging of each point to each label, b) the probability distribution function (PDF) of the measured values (intensity) for each label at each point, and c) the probability computed with the help of neighbourhood functions with relation to local spatial relationships between labelled structures calculated by modelling the segmentation as an anisotropic nonstationary Markov random field. Using the first and second probabilities, an initial segmentation is generated. Utilising the neighbourhood function in Bayesian framework, the segmentation is updated iteratively until the labels of the voxels do not change. The details are fully described elsewhere (Fischl et al. 2002). Freesurfer segmentation v6.0.0 was applied here as a comparison to our proposed method.

2.4. Proposed method

The overall flowchart of our method is provided in Figure 1. First, the target image was corrected for bias, filed, and simultaneously its CSF (CerebroSpinal Fluid) map was

Table 1. Summary of the selected MRI dataset, including the ADNI subject ID, the MMSE score of the participant, his/her age, and gender, as well as the strength of the MRI scanner.

Subject ID	MMSE	Age, Sex	MRI	Subject ID	MMSE	Age, Sex	MRI
Normal Control							
ADNI_011_S_0016	28	65,M	SIEMENS 1.5T	**ADNI_073_S_0089**	30	65,M	SIEMENS 1.5T
ADNI_020_S_1288	30	59,M	SIEMENS 3T	**ADNI_100_S_1286**	30	75,F	PHILIPS 1.5T
ADNI_032_S_0479	30	73,F	SIEMENS 3T	**ADNI_018_S_0425**	29	85,M	PHILIPS 3T
ADNI_127_S_0260	30	78,F	GE 3T	**ADNI_023_S_0031**	30	77,F	SIEMENS 3T
ADNI_009_S_0842	28	73,M	GE 1.5T	**ADNI_023_S_0061**	29	77,F	SIEMENS 3T
ADNI_011_S_0021	30	72,F	SIEMENS 3T	**ADNI_037_S_0303**	29	84,M	SIEMENS 3T
MCI							
ADNI_002_S_0729	27	65,F	PHILIPS 3T	**ADNI_003_S_1057**	26	61,F	SIEMENS 1.5T
ADNI_011_S_0856	27	60,M	SIEMENS 1.5T	**ADNI_011_S_0241**	27	81,M	SIEMENS 1.5T
ADNI_016_S_1138	27	67,M	SIEMENS 3T	**ADNI_012_S_1292**	26	76,M	PHILIPS 3T
ADNI_023_S_0331	27	64,F	SIEMENS 3T	**ADNI_013_S_0325**	28	70,F	SIEMENS 1.5T
ADNI_002_S_1070	25	73,M	PHILIPS 3T	**ADNI_100_S_0892**	28	72,F	PHILIPS 1.5T
ADNI_002_S_0954	25	69,F	GE 1.5T	**ADNI_123_S_0108**	27	78,M	PHILIPS 1.5T
AD							
ADNI_005_S_0221	20	67,M	GE 1.5T	**ADNI_126_S_0606**	23	68,F	GE 3T
ADNI_016_S_1263	26	64,F	SIEMENS 1.5T	**ADNI_100_S_1062**	24	82,M	PHILIPS 1.5T
ADNI_023_S_0139	25	65,F	SIEMENS 3T	**ADNI_002_S_0816**	26	70,M	GE 1.5T
ADNI_067_S_1185	20	62,M	SIEMENS 3T	**ADNI_009_S_1334**	24	64,M	GE 1.5T
ADNI_023_S_1289	20	77,F	SIEMENS 3T	**ADNI_027_S_1385**	26	69,F	SIEMENS 3T
ADNI_082_S_1079	20	78,M	SIEMENS 3T	**ADNI_098_S_0149**	20	87,M	GE 1.5T

extracted using SPM12 (http://www.fil.ion.ucl.ac.uk/spm/software/). Since intensity non-uniformity (INU) in MR images is a major issue when conducting analysis of brain structural properties, optimised parameters were used in SPM12 (Ganzetti et al. 2016). Using FSL v5.0.9 (https://fsl.fmrib.ox.ac.uk/fsl/) and the Brain Extraction Tool (BET) (Smith 2002), non-brain tissue from the target image were removed. The intensity inhomogeneity corrected image was then registered with linear affine transformation and a non-linear transformation, to the MNI-ICBM152 v.2009c nonlinear symmetric space, with 1x1x1 mm3 resolution.

The registration was performed by cross correlation as the similarity index and through usage of the ANTs (Advanced Normalisation Tools) toolkit which utilises the symmetric normalisation methodology (SyN) (Avants et al. 2008). The left and right hippocampus ROIs (Region of Interest) in the MNI-ICBM152 v.2009c space which are labelled according to the HarP were then back registered to the target space by applying inverse transformations. Error correction was applied to the ROIs by subtracting the CSF map of the target image from the hippocampus ROIs. This mask, which we call PI (Prior Information), was the input for the segmentation algorithm.

As the border of hippocampus with the nearby structures, such as amygdala, is not very clear in parts of the image and the two structures may have a similar MRI intensity, the segmentation algorithm had trouble being applied there. Therefore, these areas had to be identified. For this purpose, we constructed a binary map which contained the gradient information of the target image inside the hippocampus ROIs. First, the gradient magnitude of the whole image was computed, considering this map as G(Img). Next, the gradient inside the hippocampus ROIs were obtained through the usage of:

$$G(PI) = G(Img) \cap PI \tag{1}$$

In order to create the binary map from G(PI), we used a threshold which divided the voxels from PI into edge and non-edge voxels. The value for thresholding was adjusted based on the image, and the binary map was defined as follows:

$$Gb(PI) = \begin{cases} 0 \text{ for } G(PI) < threshold \\ 1 \text{ for } G(PI) > threshold \end{cases} \tag{2}$$

In Figure 2, the Gb(PI) map for one sagittal slice is demonstrated. As this figure shows, the border between the hippocampus and amygdala has the value of zero. This binary map is later used for locally integrating the prior information into the level set formulation.

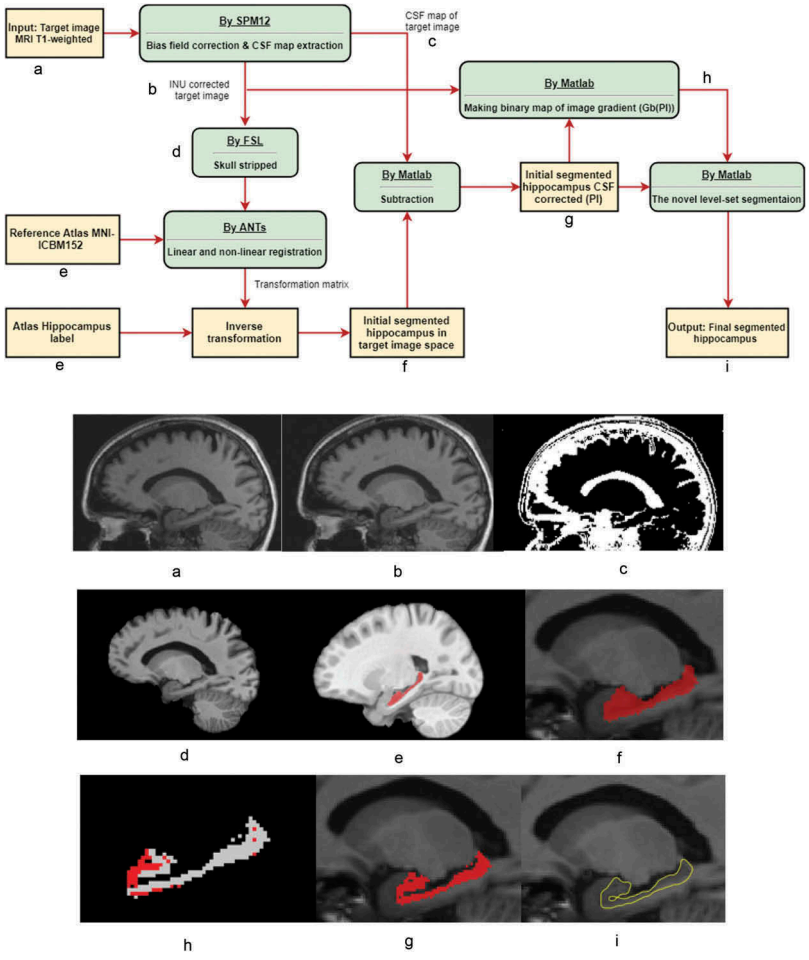

Figure 1. The summarised flowchart of our proposed method for hippocampus segmentation and a demonstration of the outputs of each step. (a): T1-weighted input image, (b): input image after correction for intensity non-uniformity, (c): CSF map of the input image, (d): skull stripped image of image (b), (e): MNI-ICBM152 atlas with segmented hippocampus based on HarP, (f): initial segmented hippocampus using registration with atlas, (h): gradient binary map of image (f), (g): CSF removed from image (f); (i): the final segmented hippocampus using the proposed level set framework.

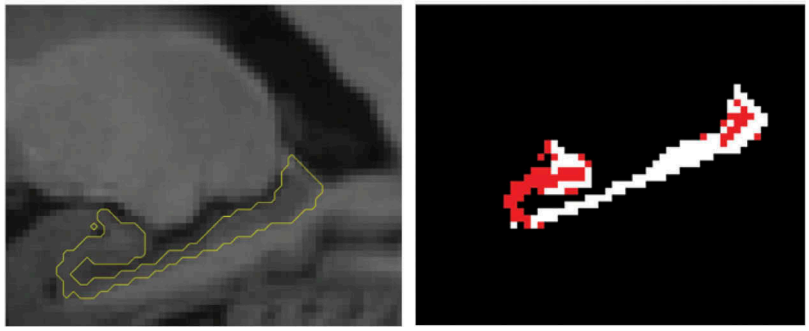

Figure 2. The estimated ROI for the hippocampus in a sagittal view of an MRI image (left); the Gb(IP) map (binary map of the gradient magnitude within the hippocampus ROI) for the corresponding image (right): red voxels represent the value of 0 in the map, and white voxels represent the value of 1.

For segmentation, in the final step, we used a novel level set method which was implemented in Matlab v.8.5 on a laptop with Intel Corei5, 3.2 GHz CPU, 6 GB RAM, and Windows 10 operating system. The basic idea of the level set was to represent the curves or surfaces as the zero level set of a dimensional hyper-surface, providing the advantage of easily handling of the topological changes. Another advantage was the interface evolution being completely determined by geometrical partial differential equations (PDEs), where various forces were integrated together to advance the dynamic interface towards the optimal sites for image segmentation. Assuming Ω was a bounded open subset of R^2, $I:\Omega \to R$ being the target image, and $\phi(x,y,t)$ the level set function, the curve C was defined as:

$$\begin{cases} C = \{x \in \Omega : \ \phi(x) = 0\} \\ inside(C) = \{x \in \Omega : \ \phi(x) > 0\} \\ outside(C) = \{x \in \Omega : \ \phi(x) < 0\} \end{cases} \tag{3}$$

The general movement formula of level set (with ∇ as the gradient operator) was as follows:

$$\frac{\partial \phi}{\partial t} + \ F|\nabla \phi| = 0 \tag{4}$$

where F is the speed function that relates to evolving surface characteristics (e.g. normal direction, curvature, etc.) and image characteristics (e.g. grey level, gradient). Due to the aim of this study, we chose a level set method which dynamically used the global and local information, and could therefore deal with challenges in hippocampus segmentation, such as intensity inhomogeneity and weak and blurred boundaries. To accomplish this, we integrated the SBGFRLS (Selective Binary and Gaussian Filtering Regularised Level Set) (Zhang et al. 2010) and LAC (Localising Region-Based Active Contours) (Lankton and Tannenbaum 2008) models. In traditional level set methods, the level set function is initialised to be a Signed Distance Function (SDF) and should be re-initialised during the evolution, which has disadvantages such as moving the zero level set away from its inference and the expensive computation needed for the re-initialising step. Alternatively, utilising the SBGFRLS technique, the level set function is initialised with a binary function and a Gaussian filter is utilised to regularise it after each iteration. The strength of the regularisation is controlled by the standard deviation of the Gaussian filter. In this study, we used both local and global intensity information in order to develop a Hybrid Region-based Sign Pressure Force (HSPF) function, as proposed previously (Zhang et al. 2017). The local SPF function was defined as:

$$L(I(x)) = \frac{I(x) - \frac{u_1(x)+u_2(x)}{2}}{max\left(\left|I(x) - \frac{u_1(x)+u_2(x)}{2}\right|\right)} \ x \ \in \Omega \tag{5}$$

where $u_1(x)$ and $u_2(x)$ are the mean values of the intensity inside and outside the contour localised by a window at the point x, which are computed according to a previous method (Lankton and Tannenbaum 2008). The global SPF (Sign Pressure Force) function is defined as:

$$G(I(x)) = \frac{I(x) - \frac{c_1(x)+c_2(x)}{2}}{max\left(\left|I(x) - \frac{c_1(x)+c_2(x)}{2}\right|\right)} \ x \in \Omega \tag{6}$$

where $c_1(x)$ and $c_2(x)$ represent the intensity averages of regions inside and outside the contour, computed according to (Zhang et al. 2010). The hybrid SPF function is defined as follows (Zhang et al. 2017):

$$HSPF = \ w(x)G(I(x)) + (1 - w(x))L(I(x)) \ x \in \Omega \tag{7}$$

In Equation (7), w(x) is a weighted function that decides which SPF function has a higher dynamic effect on the segmentation. It is computed as follows (Dong et al. 2013):

$$w(x) = \lambda.average(C_N).(1 - C_N) \ x \in \Omega \tag{8}$$

in which λ is a fixed positive parameter, and average (C_N) represents overall contrast information of the image. Additionally, C_N is the local contrast ratio of the image, defined as:

$$C_N = \frac{M_{max} - M_{min}}{M_g} \tag{9}$$

N denotes the size of local window, with M_{max} and M_{min} being the maximum and minimum of the image intensity in this local window. M_g is defined as the intensity level of the image. The value of w(x) decreases when the contour is close to the desired boundary, making the local term dominant. The value of w(x) increases when the contour is far from the desired boundary, making the global term

dominant. We used Gb(PI) as the share of prior term, PI(x), in our final evolution equation. The final evolution of level set function ϕ is defined as:

$$\frac{\partial \phi}{\partial t} = Gb(PI)\left[HSPF(I(x))\left(div\frac{\nabla\phi}{|\nabla\phi|}+\alpha\right)|\nabla\phi| + \nabla HSPF(I(x))\nabla\phi\right] + (1-Gb(PI))[PI(x)\delta(\phi)],\ \ x\in\Omega \tag{10}$$

where δ is the Dirac function and $div\frac{\nabla\phi}{|\nabla\phi|}\left(divergence\frac{\nabla\phi}{|\nabla\phi|}\right)$ represents the curvature of the level set function and αcontrols the shrinking or expanding speed when the contour is outside or inside the desired boundary. As indicated in Figure 1, the input of the segmentation step is a CSF corrected hippocampus ROI in the target image which is obtained from the previous steps. The output is the final ROI hippocampus. Through this, the proposed level set method achieves superior segmentation performance in terms of accuracy and robustness (Zhang et al. 2017). Through usage of its special feature of dynamically using local and global information, if the initial hippocampus contour is already near the desired boundary, the local force will be active and the contour in these points will be adjusted based on the target image information. If the initial hippocampus contour is far from the desired boundary at some points in contour, the level set formulisation will allow the global force to be activated. According to Equation (8), in voxels where the gradient is very low, the binary map is equal to zero, and therefore the prior information plays an effective role. The parameters for our level set implementation are as follows: threshold for binary map: 90, window size of the Gaussian filtering kernel: 3, standard deviation of the Gaussian filtering: 2, time step for evolution of level set function ϕ: 0.5, number of iteration for evolution of level set function ϕ: 60, local window size for local SPF function: 5, local window size of the local contrast ratio: 5, λ in the weighted function w(x): 0.5, and α in the final evolution of level set function: 3. For qualitative comparison for the segmentation results of our proposed method and Freesurfer, a 3D view of a left hippocampus of one typical subject is illustrated in Figure 3.

3. Results

3.1. Volumetric analysis

Table 2 provides the results of hippocampus volumetric analysis of the 36 MRI data obtained from the ADNI-HarP dataset. Three volumetric methods were applied to each image: Freesurfer v.6, our proposed method, and the ground truth approach, which was a manual segmentation based on HarP. Freesurfer returned the average hippocampal volumes in the right and left hemispheres as 3257.42 ± 615 and 3266.61 ± 654.7 mm^3, respectively. Our proposed method showed these values to be 2659.69 ± 622.5 and 2535.33 ± 599.1 mm^3, whereas the ground truth approach measurements were 2659.83 ± 574.3 and 2585.33 ± 546.4 mm^3.

3.2. Accuracy tests

A number of different approaches were utilised to compare the results of the three methods. First, Intra-class correlation coefficient (ICC two-way mixed) was used (Shrout and Fleiss 1979), using IBM Statistics SPSS v.22. As shown in Figure 4, the results of Freesurfer, as well as our proposed approach, were contrasted to the results of manual segmentation. For comparison, we also computed ICC between Freesurfer and our proposed method.

For the right hemisphere measurements, the ICCs for the results of Freesurfer and our method versus manual segmentation were 0.96 and 0.973, respectively, and the values for the left hemisphere were 0.925 and 0.970. The ICCs for the results of Freesurfer versus our method were 0.955 and 0.891 for right and left hemisphere, respectively. According to the plots, an overestimated bias for Freesurfer can be observed related to both ground truth and our method. The results show that, although our method and Freesurfer had consistency, there was higher consistency between our method and manual segmentation.

Second, we used a Bland–Altman plot (Bland and Altman 1999), a graphical method to assess the level of agreement between measurements. These plots are illustrated in Figure 5. The red line shows the average of the differences between the measurements of the two methods. The green lines are calculated as the average mean differences plus 1.96 times the standard deviation of the differences. Based on these plots, there is a tendency for overestimation in Freesurfer and the results of our method showed more similarity to the ground truth as the red line in the Bland–Altman plot is almost zero with narrower limit space between red and green lines in our method.

Third, we computed overlap measurements. Two of the most frequently used coefficients in this regard are Dice Similarity Coefficient (DSC) (Dice 1945), and the Jaccard Index (JI) (Jaccard 1912). Both Dice and JI have output values between 0 and 1, with a value of 1 signifying perfect overlapping, and a value of 0 showing no common pixels between the two images.

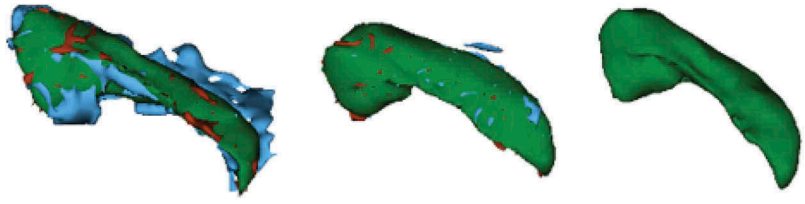

Figure 3. The ROIs extracted for the left hippocampus in a sample data, in the three approaches: FreeSurfer (left), our approach (middle), and the gold standard (right). Green colour represents true positive voxels, the blue colour represents false positives, and the red colour shows false negative voxels, as compared with the ground truth.

Table 2. The results of hippocampus volumetry in the whole dataset, using the three approaches: Freesurfer, our proposed method, and the ground truth. The average (and standard deviation) of the volumes in each group (NC, MCI, AD), as well as for all datasets are also provided. The volumes are in cubic millimetres.

	FreeSurfer		Proposed method		Ground truth	
Subject ID	Right Hippocampus	Left Hippocampus	Right Hippocampus	Left Hippocampus	Right Hippocampus	Left Hippocampus
			Normal Control			
ADNI_127_S_0260	3201	2996	2694	2638	2865	2715
ADNI_011_S_0016	3652	3687	2936	2885	2990	2798
ADNI_020_S_1288	4737	4466	3743	3429	3791	3509
ADNI_032_S_0479	3537	4300	3035	3421	3203	3403
ADNI_009_S_0842	4181	3690	3469	3337	3330	3243
ADNI_011_S_0021	3778	3829	3194	3145	3195	3144
ADNI_073_S_0089	3821	4013	3031	3104	3207	3352
ADNI_100_S_1286	4471	4298	3669	3478	3588	3557
ADNI_018_S_0425	2890	3047	2339	2344	2692	2714
ADNI_023_S_0031	3435	3796	2801	3039	2795	2951
ADNI_023_S_0061	3690	3230	3127	2713	3198	2790
ADNI_037_S_0303	3121	3141	2540	2561	2534	2629
AVERAGE ± STD	**3709.5 ± 544**	**3707.75 ± 512**	**3048.20 ± 430**	**3007.83 ± 380**	**3115.66 ± 363**	**3067.08 ± 340**
			MCI			
ADNI_002_S_0729	3523	2891	2510	2117	2341	1906
ADNI_011_S_0856	3539	3617	3200	2607	3003	2905
ADNI_016_S_1138	3402	3023	2919	2602	2713	2433
ADNI_023_S_0331	3295	3293	2759	2433	2233	2160
ADNI_002_S_1070	4150	4001	4325	4157	3878	3636
ADNI_002_S_0954	2824	2463	2053	1901	2073	1876
ADNI_003_S_1057	3348	3543	2657	2796	2687	2799
ADNI_011_S_0241	2532	3113	1991	2558	2057	2677
ADNI_012_S_1292	3451	4452	2354	2130	2715	2578
ADNI_013_S_0325	2444	2240	2151	1875	2182	1946
ADNI_100_S_0892	2818	2711	1841	2157	2032	2214
ADNI_123_S_0108	3710	3600	3275	3053	3196	2965
AVERAGE ± STD	**3253 ± 503**	**3245.60 ± 638**	**2669.60 ± 699**	**2532.16 ± 625**	**2592.5 ± 560**	**2507.91 ± 526**
			AD			
ADNI_005_S_0221	2504	2473	2147	1809	2375	2017
ADNI_016_S_1263	2642	2342	2054	1977	2133	1994
ADNI_023_S_0139	2614	2810	2322	2387	2275	2284
ADNI_067_S_1185	3137	2550	2251	1955	2521	2248
ADNI_023_S_1289	2275	2428	1554	1755	1468	1766
ADNI_082_S_1079	2521	2499	2442	1679	2232	1966
ADNI_126_S_0606	2358	2942	1751	2261	1824	2139
ADNI_100_S_1062	3248	3090	3083	2045	2916	2426
ADNI_002_S_0816	3598	3218	2860	2430	2805	2482
ADNI_009_S_1334	3309	3912	2575	2375	2761	2584
ADNI_027_S_1385	2296	2227	1626	1492	1642	1542
ADNI_098_S_0149	3215	3667	2471	2627	2304	2724
AVERAGE ± STD	**2809.75 ± 460**	**2846.5 ± 537**	**2261.33 ± 470**	**2066 ± 349**	**2271.33 ± 454**	**2181 ± 345**
OVERAL AVERAGE ± STD	**3257.42 ± 615**	**3266.61 ± 654.7**	**2659.69 ± 622.5**	**2535.33 ± 599.1**	**2659.83 ± 574.3**	**2585.33 ± 546.4**

Table 3 provides the results of these two tests. As it is illustrated, all the Dice and JI values for both the right and left hippocampus volumes were higher when contrasting our method versus the ground truth, compared to Freesurfer, which is another indication of the higher accuracy of our method.

3.3. Classification

For inspecting the effects of demographic information between NC vs MCI group and NC vs AD group, we applied independent samples t-test for age (continuous variable) and chi-square test for sex and scanner strength (categorical variables) using IBM Statistics SPSS v.22. The summary of dataset information is provided in Table 4. According to the results, the computed p-values were greater than 0.05; therefore, it presents no significant differences for those factors in NC vs MCI group, as well as NC vs AD group.

For classification purposes, a linear discriminator was applied in SPSS. We used volumes obtained from Freesurfer, our method and manual segmentation (HarP). In order to decrease the variability of the hippocampus volume measurements, all volumes were normalised with intracranial volume (ICV) computed by Freesurfer, and then the left and right hippocampus volumes were averaged. Sensitivity, specificity and accuracy were computed in two cases of classification: NC vs AD and NC vs MCI. The results are listed in Table 5.

4. Discussion

For manual hippocampus segmentation, the expert is knowledgeable about the location and shape of this structure in the brain. Utilising this pre-existing knowledge in combination with the information from the target image which is generally the intensity values, he/she would be able to define the borders of the hippocampus in each slice. However, in certain situations such as between hippocampus and the amygdala, identifying the borders of hippocampus is very complicated. In these situations, the expert has to rely on his/her prior knowledge

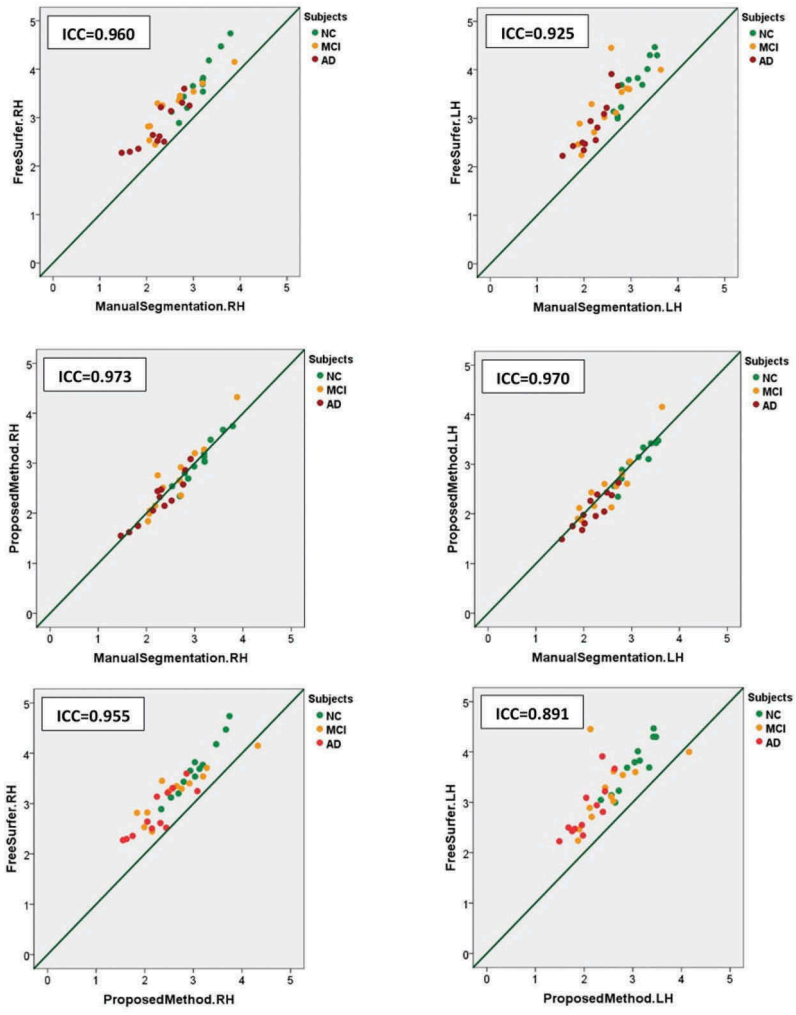

Figure 4. The results of the Intra-Class Correlation (ICC) between the results of our method versus the ground truth, Freesurfer versus the ground truth, as well as Freesurfer versus our method. The first row illustrates the ICCs between the FreeSurfer and ground truth, for the right and left hippocampus, the second row represents the same values for our proposed approach and the third row represents ICCs between our method and Freesurfer. The green line is the unity line, and the hippocampus volumes are reported in cubic centimetres.

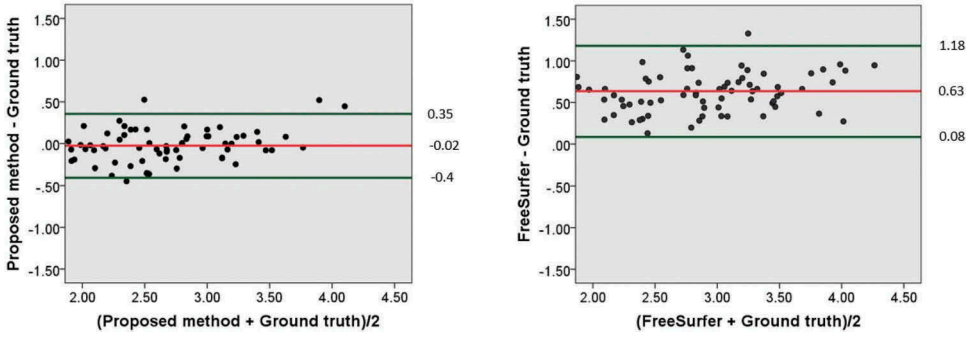

Figure 5. The results of the Bland–Altman plots for the results of our proposed method versus ground truth (left), and for the Freesurfer results versus ground truth (right). The red lines represent mean values of the differences, and the green lines represent 1.96 times the standard deviation of the differences.

about the shape and location of the hippocampus. In our proposed method, we tried to implement the described manual segmentation procedure. We obtained the prior knowledge from a simple registration step, improving its performance by CSF removal. The obtained ROI was used for automatically initialising the level set algorithm. Our segmentation used a hybrid SPF function, which adaptively utilised the local and global region information. Local information helped to overcome the intensity inhomogeneity of MR images. Global information helped to avoid the contour stopping at the local minima. For situations where the image alone does not provide sufficient information for the segmentation, for instance

Table 3. The results of Dice similarity and Jaccard index values, for the Freesurfer and our method, versus the ground truth. Average values and standard deviations of these measurements for each group (NC, MCI, AD) as well as for all datasets for the left and right Hippocampus are listed.

	FreeSurfer				Proposed Method			
	Right Hippocampus		Left Hippocampus		Right Hippocampus		Left Hippocampus	
Subject ID	Dice	JI	Dice	JI	Dice	JI	Dice	JI
				Normal Control				
ADNI_127_S_0260	0.786	0.648	0.793	0.658	0.895	0.811	0.885	0.795
ADNI_011_S_0016	0.774	0.632	0.762	0.616	0.862	0.757	0.861	0.756
ADNI_020_S_1288	0.778	0.637	0.760	0.613	0.885	0.793	0.868	0.767
ADNI_032_S_0479	0.789	0.652	0.771	0.628	0.875	0.777	0.881	0.787
ADNI_009_S_0842	0.740	0.587	0.766	0.621	0.862	0.758	0.872	0.774
ADNI_011_S_0021	0.795	0.660	0.803	0.671	0.885	0.750	0.906	0.828
ADNI_073_S_0089	0.767	0.622	0.785	0.646	0.863	0.760	0.857	0.750
ADNI_100_S_1286	0.790	0.652	0.773	0.630	0.883	0.791	0.875	0.778
ADNI_018_S_0425	0.812	0.684	0.796	0.661	0.874	0.776	0.852	0.743
ADNI_023_S_0031	0.772	0.629	0.746	0.595	0.841	0.726	0.861	0.757
ADNI_023_S_0061	0.792	0.656	0.739	0.585	0.873	0.774	0.855	0.747
ADNI_037_S_0303	0.770	0.627	0.760	0.613	0.867	0.765	0.877	0.780
AVERAGE ± STD	**0.780 ± 0.02**	**0.640 ± 0.02**	**0.771 ± 0.02**	**0.628 ± 0.03**	**0.872 ± 0.01**	**0.770 ± 0.02**	**0.871 ± 0.01**	**0.772 ± 0.02**
				MCI				
ADNI_002_S_0729	0.722	0.566	0.659	0.492	0.841	0.726	0.819	0.685
ADNI_011_S_0856	0.771	0.629	0.737	0.584	0.863	0.760	0.839	0.723
ADNI_016_S_1138	0.746	0.595	0.758	0.611	0.895	0.810	0.892	0.806
ADNI_023_S_0331	0.714	0.555	0.681	0.517	0.839	0.723	0.823	0.700
ADNI_002_S_1070	0.799	0.666	0.788	0.650	0.875	0.777	0.854	0.745
ADNI_002_S_0954	0.726	0.570	0.725	0.569	0.842	0.727	0.815	0.688
ADNI_003_S_1057	0.762	0.615	0.745	0.593	0.831	0.711	0.849	0.737
ADNI_011_S_0241	0.678	0.512	0.755	0.606	0.811	0.682	0.815	0.688
ADNI_012_S_1292	0.697	0.535	0.636	0.467	0.858	0.751	0.806	0.675
ADNI_013_S_0325	0.759	0.612	0.732	0.577	0.863	0.759	0.822	0.698
ADNI_100_S_0892	0.644	0.475	0.719	0.561	0.816	0.690	0.839	0.723
ADNI_123_S_0108	0.770	0.626	0.759	0.611	0.867	0.765	0.828	0.707
AVERAGE ± STD	**0.732 ± 0.04**	**0.580 ± 0.05**	**0.724 ± 0.04**	**0.570 ± 0.05**	**0.850 ± 0.02**	**0.740 ± 0.04**	**0.833 ± 0.02**	**0.714 ± 0.04**
				AD				
ADNI_005_S_0221	0.764	0.619	0.647	0.479	0.821	0.697	0.796	0.662
ADNI_016_S_1263	0.707	0.547	0.740	0.588	0.826	0.704	0.811	0.682
ADNI_023_S_0139	0.761	0.615	0.745	0.594	0.851	0.740	0.851	0.741
ADNI_067_S_1185	0.721	0.564	0.712	0.553	0.829	0.708	0.803	0.671
ADNI_023_S_1289	0.682	0.517	0.703	0.542	0.833	0.714	0.838	0.722
ADNI_082_S_1079	0.725	0.569	0.675	0.510	0.804	0.672	0.801	0.668
ADNI_126_S_0606	0.712	0.553	0.702	0.541	0.823	0.699	0.834	0.715
ADNI_100_S_1062	0.782	0.641	0.726	0.570	0.841	0.726	0.802	0.669
ADNI_002_S_0816	0.754	0.605	0.748	0.598	0.865	0.762	0.822	0.698
ADNI_009_S_1334	0.725	0.568	0.645	0.476	0.829	0.707	0.829	0.707
ADNI_027_S_1385	0.703	0.542	0.720	0.653	0.840	0.724	0.855	0.747
ADNI_098_S_0149	0.718	0.560	0.734	0.580	0.839	0.723	0.852	0.742
AVERAGE ± STD	**0.730 ± 0.03**	**0.575 ± 0.04**	**0.708 ± 0.03**	**0.560 ± 0.05**	**0.833 ± 0.01**	**0.715 ± 0.02**	**0.824 ± 0.02**	**0.702 ± 0.03**
OVERAL AVERAGE± STD	**0.747 ± 0.04**	**0.598 ± 0.05**	**0.735 ± 0.04**	**0.585 ± 0.05**	**0.852 ± 0.02**	**0.741 ± 0.03**	**0.843 ± 0.03**	**0.730 ± 0.04**

Table 4. Demographic details and scanner strength of the selected MRI dataset for classification.

Groups	NC	MCI	AD
Number of subjects	12	12	12
Age in years (average ± SD)	73.6 ± 7.6	69.7 ± 6.6	71.1 ± 8
Gender Male (%)	6(50%)	6(50%)	7(58%)
MRI strength 3T (%)	8(66%)	5(41%)	6(50%)

Table 5. Classification results in two conditions: normal control vs AD and normal control vs MCI, using the normalised hippocampus volume computed by HarP, our method, and Freesurfer.

Groups	Method	Sensitivity	Specificity	Accuracy
NC vs AD	Freesurfer	83%	83%	83%
	HarP	91%	91%	91%
	Proposed method	91%	91%	91%
NC vs MCI	Freesurfer	58%	83%	70%
	HarP	75%	83%	79%
	Proposed method	66%	83%	75%

between hippocampus and amygdala, our method mostly relies on prior information. In addition, our method is more robust when subject to re-initialisation or regularisation compared to conventional level set methods due to the use of a Gaussian convolution kernel for regularisation. In brief, this study proposed a new approach for hippocampus segmentation without requiring multiple registration, training data, or learning steps, which is therefore more simple to replicate. In addition, the accuracy of our method was acceptable.

There are a few studies which have used local weighting in a level set method for hippocampus segmentation (Zarpalas et al. 2014; Achuthan and Rajeswari 2015). In a previous study (Zarpalas et al. 2014), a hybrid ACM with OLMs & multi-atlas with joint label fusion was proposed which utilised the learning procedure and multi-atlas steps, which were relatively complicated to apply, and were time-consuming. Furthermore, the mean dice was reported at around 0.86. In another study

(Achuthan and Rajeswari 2015), a locally weighted Prior based Level Set (LocPLS) was used and the level set was a GAC model. The mean dice was reported at 0.81. In the current study, we have used locally weighted prior knowledge in a novel level-set method, based on hybrid SPF function, which produced an average dice index of around 0.85. Our method in comparison to a previous one (Zarpalas et al. 2014) is much simpler to implement and requires less time, while producing comparable outcomes despite one registration step and no learning procedure. The CSF correction step was performed in order to enhance the accuracy of our method.

It is worth noting that we compared our results with Freesurfer because this package is a benchmark and widely used software, developed to segment cortical and subcortical brain structures using multiple segmentation frameworks. To compare our results with those obtained from Freesurfer, we used a number of statistical approaches, with the manual hippocampus segmentation being the gold standard. The average of Dice and Jaccard indices in both left and right hippocampus for our method compared to the gold standard were 0.8475 and 0.7355, respectively, whereas these measurements for Freesurfer were 0.741 and 0.5915. Our ICC results were also superior over Freesurfer. Additionally, the Bland–Altman plot demonstrated that our method did not show obvious overestimation or underestimation in the hippocampus segmentation. Our approach achieved classification accuracies of 91% for NC vs AD and 75% for NC vs MCI which is close to the HarP classification results.

Despite the obvious strengths, this study suffered from two major limitations. First, there are some parameters in the level set method which need to be adjusted according to the target image properties. Therefore, to apply this method to a dataset which is obtained with various sequences, it might be necessary to choose different values for the parameters. We used the same parameters for all our images as mentioned at the end of section 2.4 even though the MR images were captured differently. Second, as the aim of this study was only to introduce our method, a small dataset was selected; it is necessary to replicate this method on a larger dataset of MR images with diverse characteristics to assess the feasibility of this method for clinical applications.

Disclosure statement

No potential conflict of interest was reported by the authors.

Notes on contributors

Nazanin Safavian has MSc in Biomedical engineering and she is a researcher in Neuroimaging and Analysis Group (NIAG), with her main expertise in the field of Neuroimaging and image processing.

Seyed Amir Hossein Batouli is an assistant Professor, with his main expertise in the field of Neuroimaging.

Dr. Mohammad Ali Oghabian is a full Professor of Medical Physics and a member of Scientific Board, Tehran University of Medical Sciences. He is also head of Neuroimaging and Analysis Group (NIAG), and also Biomarker imaging Group, Research Center for Molecular and Cellular Imaging, Tehran University of Medical Sciences.

References

Achuthan A, Rajeswari M. 2015. Hippocampus segmentation using locally weighted prior based level set. Seventh International Conference on Graphic and Image Processing (ICGIP 2015); Singapore. International Society for Optics and Photonics. p. 98170G.

Akhondi-asl A, Jafari-khouzani K, Elisevich K, Soltanian-zadeh H. 2011. Hippocampal volumetry for lateralization of temporal lobe epilepsy: automated versus manual methods. Neuroimage. 54:S218–S226.

Amoroso N, Errico R, Bruno S, Chincarini A, Garuccio E, Sensi F, Tangaro S, Tateo A, Bellotti R, Initiative ADN. 2015. Hippocampal unified multi-atlas network (HUMAN): protocol and scale validation of a novel segmentation tool. Phys Med Biol. 60:8851.

Anand KS, Dhikav V. 2012. Hippocampus in health and disease: an overview. Ann Indian Acad Neurol. 15:239.

Apostolova LG, Zarow C, Biado K, Hurtz S, Boccardi M, Somme J, Honarpisheh H, Blanken AE, Brook J, Tung S. 2015. Relationship between hippocampal atrophy and neuropathology markers: a 7T MRI validation study of the EADC-ADNI harmonized hippocampal segmentation protocol. Alzheimer's Dementia. 11:139–150.

Avants BB, Epstein CL, Grossman M, GEE JC. 2008. Symmetric diffeomorphic image registration with cross-correlation: evaluating automated labeling of elderly and neurodegenerative brain. Med Image Anal. 12:26–41.

Bao S, Chung AC. 2018. Multi-scale structured CNN with label consistency for brain MR image segmentation. Comput Methods Biomech Biomed Eng. 6:113–117.

Bland JM, Altman DG. 1999. Measuring agreement in method comparison studies. Stat Methods Med Res. 8:135–160.

Boccardi M, Bocchetta M, Apostolova LG, Barnes J, Bartzokis G, Corbetta G, Decarli C, Firbank M, Ganzola R, Gerritsen L. 2015a. Delphi definition of the EADC-ADNI harmonized protocol for hippocampal segmentation on magnetic resonance. Alzheimer's Dementia. 11:126–138.

Boccardi M, Bocchetta M, Morency FC, Collins DL, Nishikawa M, Ganzola R, Grothe MJ, Wolf D, Redolfi A, Pievani M. 2015b. Training labels for hippocampal segmentation based on the EADC-ADNI harmonized hippocampal protocol. Alzheimer's Dementia. 11:175–183.

Boykov Y, Veksler O, Zabih R. 2001. Fast approximate energy minimization via graph cuts. IEEE Trans Pattern Anal Mach Intell. 23:1222–1239.

Cardoso MJ, Leung K, Modat M, Keihaninejad S, Cash D, Barnes J, Fox NC, Ourselin S, Initiative ASDN. 2013. STEPS: similarity and Truth Estimation for Propagated Segmentations and its application to hippocampal segmentation and brain parcelation. Med Image Anal. 17:671–684.

Caselles V, Kimmel R, Sapiro G. 1997. Geodesic active contours. Int J Comput Vis. 22:61–79.

Chan TF, Vese LA. 2001. Active contours without edges. IEEE Trans Image Process. 10:266–277.

Chupin M, Hammers A, Liu RS, Colliot O, Burdett J, Bardinet E, Duncan JS, Garnero L, Lemieux L. 2009. Automatic segmentation of the hippocampus and the amygdala driven by hybrid constraints: method and validation. Neuroimage. 46:749–761.

Chupin M, Mukuna-bantumbakulu AR, Hasboun D, Bardinet E, Baillet S, Kinkingnéhun S, Lemieux L, Dubois B, Garnero L. 2007. Anatomically constrained region deformation for the automated segmentation of the hippocampus and the amygdala: method and validation on controls and patients with Alzheimer's disease. Neuroimage. 34:996–1019.

Collins DL, Evans AC. 1997. Animal: validation and applications of nonlinear registration-based segmentation. Int J Pattern Recognit Artif Intell. 11:1271–1294.

Collins DL, Pruessner JC. 2010. Towards accurate, automatic segmentation of the hippocampus and amygdala from MRI by augmenting ANIMAL with a template library and label fusion. Neuroimage. 52:1355–1366.

Coupé P, Manjón JV, Fonov V, Pruessner J, Robles M, Collins DL. 2011. Patch-based segmentation using expert priors: application to hippocampus and ventricle segmentation. NeuroImage. 54:940–954.

Csernansky JG, Joshi S, Wang L, Haller JW, Gado M, Miller JP, Grenander U, Miller MI. 1998. Hippocampal morphometry in schizophrenia by high dimensional brain mapping. ProcNatl Acad Sci USA, 95, p. 11406–11411.

Dice LR. 1945. Measures of the amount of ecologic association between species. Ecology. 26:297–302.

Dill V, Franco AR, Pinho MS. 2015. Automated methods for hippocampus segmentation: the evolution and a review of the state of the art. Neuroinformatics. 13:133–150.

Dolz J, Massoptier L, Vermandel M. 2015. Segmentation algorithms of subcortical brain structures on MRI for radiotherapy and radiosurgery: a survey. IRBM. 36:200–212.

Dong F, Chen Z, Wang J. 2013. A new level set method for inhomogeneous image segmentation. Image Vis Comput. 31:809–822.

Fischl B, Salat DH, Busa E, Albert M, Dieterich M, Haselgrove C, van der kouwe A, Killiany R, Kennedy D, Klaveness S. 2002. Whole brain segmentation: automated labeling of neuroanatomical structures in the human brain. Neuron. 33:341–355.

Frisoni GB, Jack CR, Bocchetta M, Bauer C, Frederiksen KS, Liu Y, Preboske G, Swihart T, Blair M, Cavedo E. 2015. The EADC-ADNI harmonized protocol for manual hippocampal segmentation on magnetic resonance: evidence of validity. Alzheimer's Dementia. 11:111–125.

Ganzetti M, Wenderoth N, Mantini D. 2016. Intensity inhomogeneity correction of structural MR images: a data-driven approach to define input algorithm parameters. Front Neuroinform. 10:10.

Geuze E, Vermetten E, Bremner J. 2005. MR-based in vivo hippocampal volumetrics: 2. Findings in neuropsychiatric disorders. Mol Psychiatry. 10:160.

Haller JW, Banerjee A, Christensen GE, Gado M, Joshi S, Miller MI, Sheline Y, Vannier MW, Csernansky JG. 1997. Three-dimensional hippocampal MR morphometry with high-dimensional transformation of a neuroanatomic atlas. Radiology. 202:504–510.

Hao Y, Wang T, Zhang X, Duan Y, Yu C, Jiang T, Fan Y, Initiative ASDN. 2014. Local label learning (LLL) for subcortical structure segmentation: application to hippocampus segmentation. Hum Brain Mapp. 35:2674–2697.

Heckemann RA, Hajnal JV, Aljabar P, Rueckert D, Hammers A. 2006. Automatic anatomical brain MRI segmentation combining label propagation and decision fusion. NeuroImage. 33:115–126.

Heckemann RA, Keihaninejad S, Aljabar P, Rueckert D, Hajnal JV, Hammers A, Initiative ASDN. 2010. Improving intersubject image registration using tissue-class information benefits robustness and accuracy of multi-atlas based anatomical segmentation. Neuroimage. 51:221–227.

Hult R. 2003. Grey-level morphology combined with an artificial neural networks approach for multimodal segmentation of the hippocampus. Image Analysis and Processing, 2003. Proceedings. 12th International Conference on Mantova, Italy; IEEE. p. 277–282.

Jaccard P. 1912. The distribution of the flora in the alpine zone. New Phytol. 11:37–50.

Jack CR, Bernstein MA, Fox NC, Thompson P, Alexander G, Harvey D, Borowski B, Britson PJ,L, Whitwell J, Ward C. 2008. The Alzheimer's disease neuroimaging initiative (ADNI): MRI methods. J Magn Reson Imaging. 27:685–691.

Kass M, Witkin A, Terzopoulos D. 1988. Snakes: active contour models. Int J Comput Vis. 1:321–331.

Khan AR, Cherbuin N, Wen W, Anstey KJ, Sachdev P, Beg MF. 2011. Optimal weights for local multi-atlas fusion using supervised learning and dynamic information (SuperDyn): validation on hippocampus segmentation. NeuroImage. 56:126–139.

Kim M, Wu G, Li W, Wang L, Son Y-D, Cho Z-H, Shen D. 2013. Automatic hippocampus segmentation of 7.0 Tesla MR images by combining multiple atlases and auto-context models. NeuroImage. 83:335–345.

Kwak K, Yoon U, Lee D-K, Kim GH, Seo SW, Na DL, Shim H-J, Lee J-M. 2013. Fully-automated approach to hippocampus segmentation using a graph-cuts algorithm combined with atlas-based segmentation and morphological opening. Magn Reson Imaging. 31:1190–1196.

Lankton S, Tannenbaum A. 2008. Localizing region-based active contours. IEEE Trans Image Process. 17:2029–2039.

Lecun Y, Bottou L, Bengio Y, Haffner P. 1998. Gradient-based learning applied to document recognition. Proc IEEE. 86:2278–2324. https://ieeexplore.ieee.org/document/726791/citations#citations.

Lötjönen JM, Wolz R, Koikkalainen JR, Thurfjell L, Waldemar G, Soininen H, Rueckert D, Initiative ASDN. 2010. Fast and robust multi-atlas segmentation of brain magnetic resonance images. Neuroimage. 49:2352–2365.

Pipitone J, Park MTM, Winterburn J, Lett TA, Lerch JP, Pruessner JC, Lepage M, Voineskos AN, Chakravarty MM, Initiative ASDN. 2014. Multi-atlas segmentation of the whole hippocampus and subfields using multiple automatically generated templates. Neuroimage. 101:494–512.

Platero C, Tobar MC. 2017. Combining a patch-based approach with a non-rigid registration-based label fusion method for the hippocampal segmentation in Alzheimer's disease. Neuroinformatics. 15:165–183.

Robitaille N, Duchesne S. 2012. Label fusion strategy selection. Int J Biomed Imaging. 2012.

Sethian JA. 1999. Level set methods and fast marching methods: evolving interfaces in computational geometry, fluid mechanics, computer vision, and materials science. Cambridge, UK: Cambridge University press.

Shen D, Moffat S, Resnick SM, Davatzikos C. 2002. Measuring size and shape of the hippocampus in MR images using a deformable shape model. Neuroimage. 15:422–434.

Shrout PE, Fleiss JL. 1979. Intraclass correlations: uses in assessing rater reliability. Psychol Bull. 86:420.

Smith SM. 2002. Fast robust automated brain extraction. Hum Brain Mapp. 17:143–155.

Tong T, Wolz R, Coupé P, Hajnal JV, Rueckert D, Initiative ASDN. 2013. Segmentation of MR images via discriminative dictionary learning and sparse coding: application to hippocampus labeling. NeuroImage. 76:11–23.

Van leemput K, Bakkour A, Benner T, Wiggins G, Wald LL, Augustinack J, Dickerson BC, Golland P, Fischl B. 2009. Automated segmentation of hippocampal subfields from ultra-high resolution in vivo MRI. Hippocampus. 19:549–557.

Yushkevich PA, Wang H, Pluta J, Das SR, Craige C, Avants BB, Weiner MW, Mueller S. 2010. Nearly automatic segmentation of hippocampal subfields in in vivo focal T2-weighted MRI. Neuroimage. 53:1208–1224.

Zandifar A, Fonov V, Coupé P, Pruessner J, Collins DL, Initiative ASDN. 2017. A comparison of accurate automatic hippocampal segmentation methods. NeuroImage. 155:383–393.

Zarpalas D, Gkontra P, Daras P, Maglaveras N. 2013. Hippocampus segmentation through gradient based reliability maps for local blending of ACM energy terms. Biomedical Imaging (ISBI), 2013 IEEE 10th International Symposium on San Francisco, CA; IEEE. p. 53–56.

Zarpalas D, Gkontra P, Daras P, Maglaveras N. 2014. Accurate and fully automatic hippocampus segmentation using subject-specific 3D optimal local maps into a hybrid active contour model. IEEE J Transl Eng Health Med. 2:1–16.

Zhang K, Zhang L, Song H, Zhou W. 2010. Active contours with selective local or global segmentation: a new formulation and level set method. Image Vis Comput. 28:668–676.

Zhang L, Peng X, Li G, Li H. 2017. A novel active contour model for image segmentation using local and global region-based information. Mach Vis Appl. 28:75–89.

Zheng Q, Fan Y. 2018. Integrating semi-supervised label propagation and random forests for multi-atlas based hippocampus segmentation. Biomedical Imaging (ISBI 2018), 2018 IEEE 15th International Symposium on Washington, DC; IEEE. p. 154–157.